

# Comportement du champ magnétique terrestre lors d'un changement de polarité Étude d'un exemple

## 3.1 Introduction à l'étude

Dans le premier chapitre nous avons vu que le champ magnétique terrestre s'est renversé de nombreuses fois au cours du temps. Il s'agit d'un phénomène géophysique parmi les plus spectaculaires mais qui reste encore aujourd'hui énigmatique. La difficulté de l'étude de ce phénomène repose sur le fait que les observations sont indirectes, la dernière inversion étant datée à 780 000 ans environ. Dès lors, plusieurs problèmes se posent. Le temps d'une inversion est relativement court, entre 5000 et 7000 ans en moyenne (Clement, 2004), ce qui, sur l'échelle des temps géologiques, représente un "instantané". S'agissant d'un phénomène global, les renversements de polarité sont utilisés par exemple comme isochrone dans la méthode de datation relative basée sur la magnétostratigraphie. L'enregistrement du champ transitionnel est donc statistiquement difficile à réaliser dans les laves car il nécessite une concomitance entre les éruptions volcaniques, phénomène chaotique, et le renversement dont la durée est très brève. Il en est de même pour les sédiments, où l'enregistrement nécessite un taux de sédimentation à la fois continu et élevé (Merrill and McFadden, 1999). La fidélité de l'enregistrement peut également être remise en cause, leur interprétation étant parfois rendue difficile par la superposition d'une (ou plusieurs) composante(s) à l'aimantation primaire. En effet, au cours d'une inversion de polarité, le champ diminue en intensité, probablement d'un facteur 10 (Prévot et al., 1985; Leonhardt and Soffel, 2002; Valet et al., 2005). L'aimantation primaire de la roche, proportionnelle à l'intensité du champ, est donc relativement faible. Par conséquent, sa conservation au cours du temps est compromise.

Plusieurs questions restent en suspens sur cette thématique comme : Quel est le

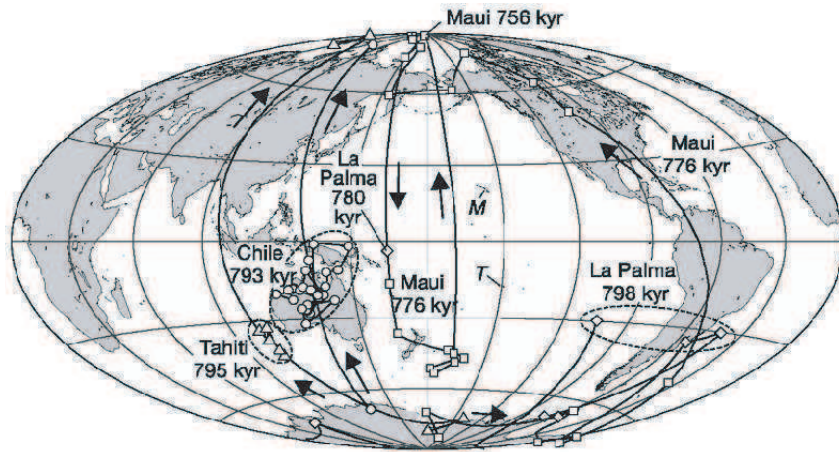


FIGURE 3.1 – PGVs pendant le renversement *Brunhes-Matuyama* (Singer et al., 2005).

devenir des composantes dipôle et non dipôle lors d'un renversement ? Quelle est la morphologie du champ transitionnel ? Existe-t-il des caractéristiques communes entre les différents renversements ? Les pôles géomagnétiques virtuels (PGV) obtenus à partir des données transitionnelles au cours des 12 derniers millions d'années semblent en partie répondre à cette dernière question. On observe un regroupement préférentiel des PGV au cours des renversements récents sur deux bandes longitudinales antipodales, l'une passant par l'Amérique et l'autre par l'Australie. En effet, les études des enregistrements sédimentaires (Clement, 1991; Laj et al., 1991) et d'autres portant sur les laves (Hoffman, 1991) montrent cette même tendance (Fig. 3.1). Ce confinement persistant sur plusieurs millions d'années, est présenté par certains comme une preuve expérimentale du couplage entre les convections nucléaires et mantelliques d'origine électromagnétique (Runcorn, 1992; Brito et al., 1999) ou thermique (Bloxham and Gubbins, 1987; Kutzner and Christensen, 2004). Toutefois, plusieurs autres études portant sur des sédiments (Vallet et al., 1992) ou des laves (Prévot and Camps, 1993), tendent à montrer au contraire que la distribution de PGV transitionnels est uniforme en longitude. Les évidences qui supportent l'hypothèse d'un couplage noyau-manteau semblent dépendre à la fois de l'intervalle de temps considéré (Camps et al., 2007) et des régions d'où proviennent les données (Hoffman et al., 2008). Il est en revanche intéressant de noter que les modèles numériques de géodynamo pour lesquels un flux de chaleur non uniforme est imposé à l'interface Noyau-Manteau simulent parfaitement l'organisation longitudinale des PGVs transitionnels (Coe et al., 2000; Kutzner and Christensen, 2004). A l'inverse, le modèle géomagnétique proposé par Leonhardt and Fabian (2007) pour le renversement Brunhes-Matuyama ne prédit pas l'existence de ces bandes longitudinales mais montre un regroupement des PGVs transitionnels dans le Pacifique. Ces questions peuvent se rattacher à l'observation de tâches de flux à la limite manteau noyau pour le champ moderne aux hautes latitudes, notamment sous l'Australie (Jackson et al., 2000; Korte and Holme,

---

2010). Ces tâches ont pu persister jusqu'au Pliocène, notamment par l'influence des hétérogénéités du manteau (Gubbins et al., 2007), voire jusqu'à la fin de l'Oligocène si l'on en croit les résultats expérimentaux d'Hoffman et al. (2008). Ainsi, des observations provenant de régions proches de l'Australie pourraient fournir des informations claires quant à une éventuelle interaction manteau-noyau.

Par ailleurs, la plupart des études montrent une diminution de l'intensité du champ dipolaire au cours du renversement ; l'intensité du champ peut décroître localement jusqu'à atteindre 10% de sa valeur initiale (Prévot et al., 1985; Leonhardt and Soffel, 2002; Valet et al., 2005, e.g.). De plus, des variations importantes des directions sont enregistrées avant (précurseur) ou au cours (rebond) du renversement (Prévot et al., 1985; Brown et al., 2004; Coe et al., 2004; Camps et al., 2011). Ces observations sont confortées par différents modèles numériques (Olson et al., 2009, 2011) et suggèrent une augmentation de la turbulence au sein du noyau liquide. Cependant, Sherwood and Shaw (1986) ont déterminé sur des laves provenant du volcan Akaroa (Nouvelle Zélande) des paléointensités transitionnelles avec une valeur significativement supérieure à celles des intensités avant et après le renversement. Si cette observation s'avère vraie, elle pose directement la question du devenir de l'amplitude de la variation séculaire pendant les renversements de polarité (Camps and Prévot, 1996). Cependant, la méthode expérimentale utilisée pour la détermination de ces paléointensités, la méthode de Shaw (1974), est extrêmement controversée par la communauté scientifique (cf. Annexe A). Un réexamen de ces données s'impose par la méthode conventionnelle de Thellier.

Dans l'optique d'apporter de nouvelles données directionnelles et de vérifier les paléointensités transitionnelles obtenues par Sherwood and Shaw (1986), nous avons ré-échantillonné le renversement enregistré dans la séquence volcanique d'Akaroa (Evans, 1970; Hoffman, 1986; Sherwood and Shaw, 1986). La mission s'est déroulée en janvier 2010 dans la Péninsule de Banks (Ile Sud de la Nouvelle Zélande, près de Christchurch). Cette péninsule est composée de deux édifices volcaniques principaux, dont Littelton forme la partie nord ouest et Akaroa la partie sud est. C'est ce dernier édifice que nous avons échantillonné. Il s'agit d'un volcan miocène formé de coulées de composition basaltique à andésitique (Stipp and McDougall, 1968; Timm et al., 2009). Nous avons prélevé près de 450 carottes et échantillonné 71 coulées sur trois sections (Fig. 3.2). La section principale LG (Lighthouse road) correspond strictement à celle qui avait été échantillonnée par Evans (1970), Hoffman (1986) and Sherwood and Shaw (1986). Nous avons choisi d'échantillonner deux nouvelles sections (SB et LA) dans l'espoir de trouver de nouvelles directions absentes de la section originale. La corrélation entre les trois sections a été réalisée sur la base d'arguments minéralogiques, géologiques (observations de terrain) et magnétique. J'ai dans un premier temps déterminé l'évolution directionnelle enregistrée

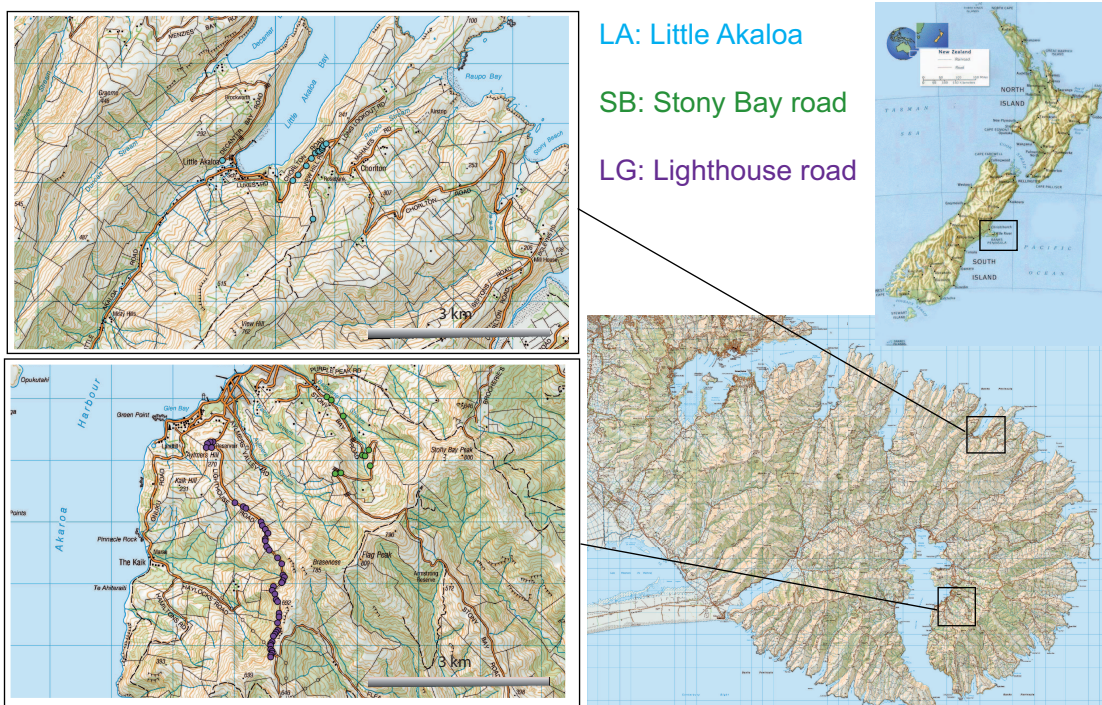


FIGURE 3.2 – Localisation de la Péninsule de Banks et des trois sections échantillonnées. Chaque point représente la localisation d'un site d'échantillonnage.

dans cette séquence volcanique. Puis, suite à une étude de la minéralogie magnétique, j'ai sélectionné les échantillons susceptibles de fournir une valeur de paléointensité par la méthode de Thellier and Thellier (1959). Malheureusement très peu d'échantillons ont rempli les critères nécessaires pour appliquer cette méthode (cf. Annexe A), dû notamment à une fraction importante de grains polydomaines dans de nombreuses coulées. De plus, la présence de titanomaghémite dans de nombreux échantillons, traduisant inévitablement la présence d'une aimantation rémanente chimique dans l'ARN, ce qui interdit toute détermination de paléointensité absolue. A la vue de cette minéralogie, j'ai décidé d'appliquer la méthode multispecimen aux échantillons présentant un comportement polydomaine et pour lesquels la nature thermo-rémanente de l'aimantation ne fait aucun doute (Dekkers and Böhnelt, 2006; Fabian and Leonhardt, 2010, cf. Chapitre 4). L'article suivant, en préparation pour être soumis à PEPI pour sa publication, résume l'ensemble des résultats et des conclusions de l'étude.

---

## 3.2 Comportement du champ magnétique lors du renversement d'Akaroa

Behavior of the transitional field during the Akaroa polarity reversal, New Zealand : low paleointensities coupled to a geomagnetic rebound ?

G. Fanjat<sup>1</sup>, P. Camps<sup>1</sup>, T. Poidras<sup>1</sup>, C. Carvallo<sup>2</sup>, B. Kennedy<sup>3</sup>, K. Hoffman<sup>4</sup>

<sup>1</sup>Géosciences Montpellier, CNRS and Université Montpellier 2, 34095 Montpellier, France.

<sup>2</sup>IMPMC, Campus Jussieu, 4 place Jussieu, 75005 Paris, France

<sup>3</sup>Physics Department, Cal Poly State University, San Luis Obispo, CA, United States

<sup>4</sup>Department of Geological Sciences, University of Canterbury, Private Bag 4800, Christchurch, New Zealand

First draft

### Abstract

We resampled a polarity reversal of late Miocene age ( $\approx 9$  Ma) recorded along a volcanic sequence in Akaroa volcano, Banks Peninsula, New Zealand. Our main objectives were twofold. First, we wanted to check the validity of old paleointensity determinations that yielded stronger values during the transitional period than during the stable periods that preceded and followed the reversal. This observation is opposite to what is generally observed from experimental determinations and numerical models. An increase in intensity during reversals would provide an extreme example of energy transfer from the axial dipole into other harmonic coefficients. However, the Shaw method, which was the experimental method used for determining these paleointensities, is strongly questioned by the scientific community. A check of these data by the conventional Thellier method was required. Second, we wanted to complete directional observations of the transitional field in order to describe the virtual geomagnetic poles (VGPs) paths during the reversal. Indeed, studies of polarity transitions of the Earth's magnetic field recorded over the past few million years, especially in Australasia, suggest a long-lived mantle control over the Earth's core, manifested by a clustering of VGPs at locations common to several younger reversal datasets from all around the globe. To achieve these two objectives, we carried out first a comprehensive magnetic mineralogy study. The directional results show a complex sequence of N-T-R-T-N-T-R polarity. The transitional VGPs obtained are clustered over two longitudinal bands : one over America and one over Australasia, in agreement with the model of mantle influence over the geodynamo during the last ten millions of

years. According to the mineralogy of the samples, we used the Thellier-Thellier's method or the multispecimen protocol to determine paleointensities. The obtained values do not confirm an increase of the intensity during the reversal. They show more scattered values of the intensity even during the stable periods, between 20 and 86  $\mu\text{T}$ , and a very low mean value, about 15  $\mu\text{T}$  before, during and after the polarity change. Based both on the field strength values and on the radiochronological ages, showing that the whole sequence was erupted in a very short time, we suggest that only the C4Ar.1n-C4Ar.1r reversal was recorded in this sequence. In this assumption, the reversal shows a complex path comparable to other reversals recorded in the northern hemisphere (for example in the Steens Mountain), including a rebound before stabilizing.

**Key words :** Magnetic Earth's reversal – Paleointensity – Australasia – Banks Peninsula

### 3.2.1 Introduction

The Earth's magnetic field resulting from the self-sustained dynamo working in the Earth's liquid outer core presents an important temporal variation range. They span from less than one year, with rapid events such as geomagnetic jerks (Mandea et al., 2010, e.g.), to several million years during which the magnetic field presents a relative stability (e.g. Jonkers et al. (2003); Pavlov and Gallet (2005)). The most impressive behavior of the Earth's magnetic field over the time are reversals, where the dipole reverses from one polarity to the opposite. The short duration of transitional field states, about few millennia (Clement, 2004), and the fragmentary nature of paleomagnetic records make difficult the study of such events. As a consequence, the field morphology during reversals is still not perfectly known and some fundamental questions remain unanswered. Does the energy of the dipole transform into that of other terms? Are there some persistent mantle-held flux concentrations at the core surface that control the behavior of the transitional field?

This last question was answered from paleomagnetic observations of transitional Virtual Geomagnetic Poles (VGPs) that seem to describe two preferred longitudinal paths, one through North and South America and the other one through Australasia. Indeed, both sedimentary records (Clement, 1991; Laj et al., 1991) and lava flow records (Hoffman, 1991; Hoffman et al., 2008) suggest such a behavior. These preferred paths are consistent during several million years, and could be explained by an interaction between the core and the mantle at the Core Mantle Boundary (CMB). Even if the geomagnetic field geometry is essentially dictated by the Earth's rotation, variations in the lower mantle and interactions with the core appear to influence the dynamo processes (Gubbins et al., 2007). Such interactions can have an electromagnetic origin (Runcorn, 1992; Brito et al., 1999) or a thermal origin (Blokhman and Gubbins, 1987; Kutzner and

### 3.2.1 Introduction

---

Christensen, 2004). Nevertheless other statistical analyses relying on sedimentary records (Valet et al., 1992) and lava flow records (Prévot and Camps, 1993) do not show this pattern. Evidences supporting a core/mantle interaction seem to be dependent of the time interval studied (Camps et al., 2007) as well as on the geographical distribution of the observations (Hoffman et al., 2008). It is interesting to note that numerical models of the geodynamo with a non uniform thermal flux at the CMB are able to reproduce the longitudinal organization of the transitional VGPs as it is assumed for a core-mantle interaction (Coe et al., 2000; Kutzner and Christensen, 2004). The geomagnetic model proposed by Leonhardt and Fabian (2007) for the Matuyama-Bruhnes reversal does not predict two longitudinal bands but shows a preference of transitional VGPs for the Pacific hemisphere. The VGP's clustering during reversals, from an experimental or a modelling point of view, is still under debate and more data are needed. This problem may be associated with concentrations of magnetic flux at the core surface at high latitudes, especially off the west coast of Australia, related to the modern field (Jackson et al., 2000; Korte and Holme, 2010). Gubbins et al. (2007) suggest that these flux patterns may have remained essentially unchanged since the Pliocene while Hoffman et al. (2008) found some evidence from a volcanic sequence in Australia for a stability of mantle control over dynamo flow since the mid-Cenozoic. Hence, analyses of transitional field behavior recorded in rocks from Australasia would be expected to provide the clearest observations about a possible core-mantle interaction.

Absolute paleointensity data show unambiguously that the field strength is considerably reduced during reversals. The local field intensity can drop below 10% of the pre-transitional value (see e.g. Prévot et al. (1985); Leonhardt and Soffel (2002); Valet et al. (2005)) and a decline of the field intensity during a pretransitional period can be described as a precursor the event (Prévot et al., 1985; Brown et al., 2004). Complex patterns also can be recorded during low field intensity transitional periods, such as aborted attempts to re-establish a stable geomagnetic field, characterized by rapid changes in the field polarity and defined as rebounds (Prévot et al., 1985; Coe et al., 2004). These observations are also supported by numerical models (Olson et al., 2009, 2011) and suggest an increase of the turbulence level within the liquid outer core during the transition. However, Sherwood and Shaw (1986) obtained stronger paleointensities in a polarity reversal recorded in a volcanic sequence at Akaroa volcano, New Zealand. In this study the experimental protocol of Shaw (1974) was used to determine the paleointensities. This observation points out directly the problem of the dipole energy during the reversal (Camps and Prévot, 1996). Indeed, an increase in magnetic field intensity during reversals would provide an extreme example of energy transfer from the axial dipole into other harmonic coefficients. Hence, a re-examination of these data by means of the conventional Thellier-Thellier method is required.

In order to provide more data on transitional directions and to check the paleointensities obtained by Sherwood and Shaw (1986), we re-sampled the Akaroa polarity reversal ( $\approx 9$  Ma). Our main objectives were twofold. The first point was to re-examine the direction, particularly the transitional ones, and the second was to determine new paleointensity data with the Thellier protocol. In the first part of this paper we report the geology and the directional data, then relying on a comprehensive rock magnetic study, we present paleointensity results from the Thellier-Thellier method and from the multispecimen pTRM method. Finally, we discuss the whole results.

### 3.2.2 Geological settings and sampling

Banks peninsula, located on the central East coast of New Zealand, South Island, South Est of Christchurch city (Fig. 3.3), comprises three main composite shield volcanoes; Akaroa and Lyttelton volcanoes which are the larger ones and the contemporaneous Mount Herber Volcanic group in the central region. They are mainly built of alkaline basaltic to andesitic lavas but pyroclastic flows are also encountered (Speight, 1924; Coombs, 1963). These volcanoes were active during the Mid- to Late-Miocene and appear to be of intraplate continental character (Weaver and Smith, 1989; Timm et al., 2009). Lyttelton volcano was active between about 12 Myrs and 10 Myrs whereas Akaroa volcano was active in a very short time interval, from 9.4 Myrs to 8.8 Myrs (Stipp and McDougall, 1968; Timm et al., 2009). Both volcanoes are preserved from tectonic event and present strong patterns of erosion (Hampton and Cole, 2009) at the origin of natural harbours in the ocean. The present diameter of Akaroa volcano is about 35 km but on basis of field observations, the original diameter was close to 50 km (Weaver and Smith, 1989). We collected samples on the Akaroa volcano along three different cross-sections: Little Akaloa, Stony Bay Road and Lighthouse Road (cf. Fig. 3.3).

We sampled in detail 51 flows along the Lighthouse road over a 480 m thick sequence, following the same section sampled by Evans (1970), Sherwood and Shaw (1986) and Hoffman (1986). We sampled also the two other sections, collecting 13 flows on 340 m high and 10 flows on 380 m high along the Little Akaloa and Stony Bay Peak sections, respectively. In total we collected 472 cores by means of a gasoline-powered portable drill. When it was possible, we collected seven cores per flow, being careful to identify landslide lenses and dikes. The lateral extension of the sampling along a flow varies from few meters to tens of meters, depending of the morphology of the outcrop. We oriented the samples using a magnetic compass corrected for local and regional anomalies by sighting either the sun at a known time or either known landmarks. In the laboratory, samples were cut into standard cylindrical paleomagnetic specimens of 1 inch in diameter and 2.2 cm-long. Then, they were stored in a null magnetic field during at least three weeks before to be analyzed. We carried out a comprehensive paleomagnetic study on these samples, relying

### 3.2.3 Paleomagnetic directions

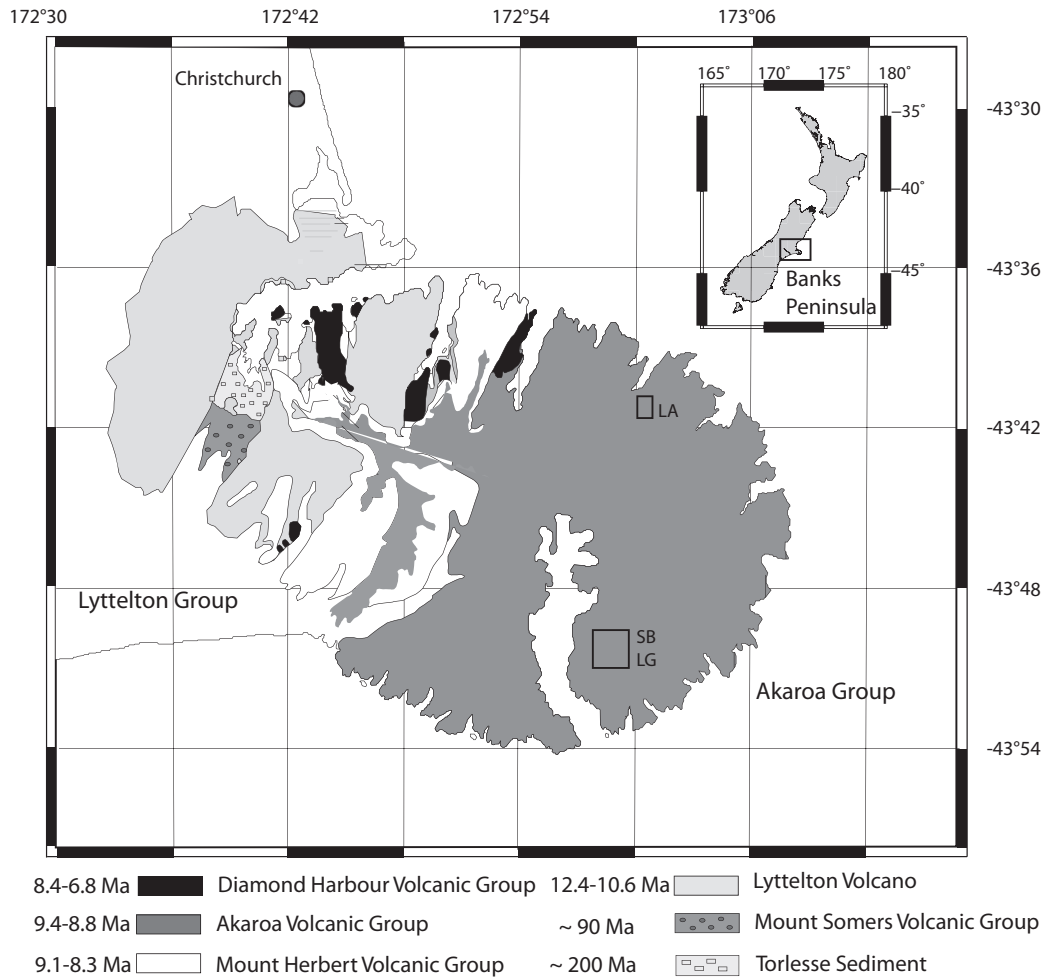


FIGURE 3.3 – Simplified geological map of Banks Peninsula. Location of the three sampled sections : Little Akaloa (LA), Light house road (LG) and Stony Bay Road (SB). Redrawn from Stipp and McDougall (1968); Timm et al. (2009)

on paleodirection measurements, rock magnetism and paleointensity determinations.

### 3.2.3 Paleomagnetic directions

#### Experimental protocol

First, we determined the 15-day magnetic viscosity index  $\nu$  (Thellier and Thellier, 1944) for the whole samples. We measured by means of a JR-5A spinner magnetometer (Agico, Czech Republic) the remanent magnetization ( $\text{NRM}_1$ ) after a two-week storage with the ambient field parallel to the positive cylinder axis of the specimen ( $\mathbf{z}$ ). Then we measured again the remanent magnetization  $\text{NRM}_2$  after a two-week storage in zero-field. The viscous index  $\nu$  is given in percent by :

$$\nu = \frac{\text{NRM}_1 - \text{NRM}_2}{\text{NRM}_2} \times 100 \quad (3.1)$$

This index can be used as a quantitative estimate of the viscous remanent magnetization (Prévot, 1981).

We used both alternative field (AF) demagnetization and thermal cleaning to determine paleodirections. For most of the flows, we demagnetized and measured in detail (15 steps up to 160 mT) one pilot sample by means of a three-axes 2G cryogenic SQUID magnetometer equipped with the 2G600 AF demagnetizer. An other pilot sample was demagnetized with thermal cleaning in a non-inductive PYROX furnace with a residual field less than 20 nT in the cooling chamber. The remanent magnetization was measured with a JR-5A spinner magnetometer after each step of demagnetization. This thermal demagnetization allows the determination of the unblocking temperatures spectrum. We choose, according to the behavior of the pilot samples, the best method to demagnetized the other samples from the same flow.

### Results

The analysis of the demagnetization diagrams was straightforward for most of the samples. Results for each flow from the three sections are presented in Tab. 3.1. We observed in most of the flows a small overprint, certainly of viscous origin. This overprint is entirely removed at 150°C. For some flows, an isothermal remanent magnetization (IRM) overprint is clearly observed, and is entirely remove between 10 and 15 mT. Nevertheless, few flows ware totally re-magnetized by IRM, probably due to lightnings and we were not able to determine any directional results. For higher AF peak values or temperature steps, we observed a perfect stability of the primary magnetization direction as shown by the straight-line decay to the origin on the vector endpoint diagrams (Fig. 3.4).

The stratigraphic relationships between the different sequences is not well established for Akaroa volcano. Nevertheless, the paleomagnetic directions obtained in the present study can perfectly be combined into a composite profile using geochemical markers, directional arguments and field observations. In order to gain in clarity, synthetic results for the three sections are summarized in Fig. 3.10. Our profile is in agreement with the ones obtained by Evans (1970) and Hoffman (1986), with a complex sequence N-T-R-T-N-T-R. We identified about ten lava flow recording a transitional field. The next step was to obtain paleointensity both from normal, reverse and transitional polarities.

#### 3.2.4 Rock magnetism properties

Paleointensity determinations by the Thellier and Thellier (1959) method present often a high failure rate. This failure is mainly due to a high number of heatings that trigger thermo-chemical alteration of magnetic minerals and changes in their magnetic properties. It is also due to the presence of multi-domain grains displaying an unwanted

### 3.2.4 Rock magnetism properties

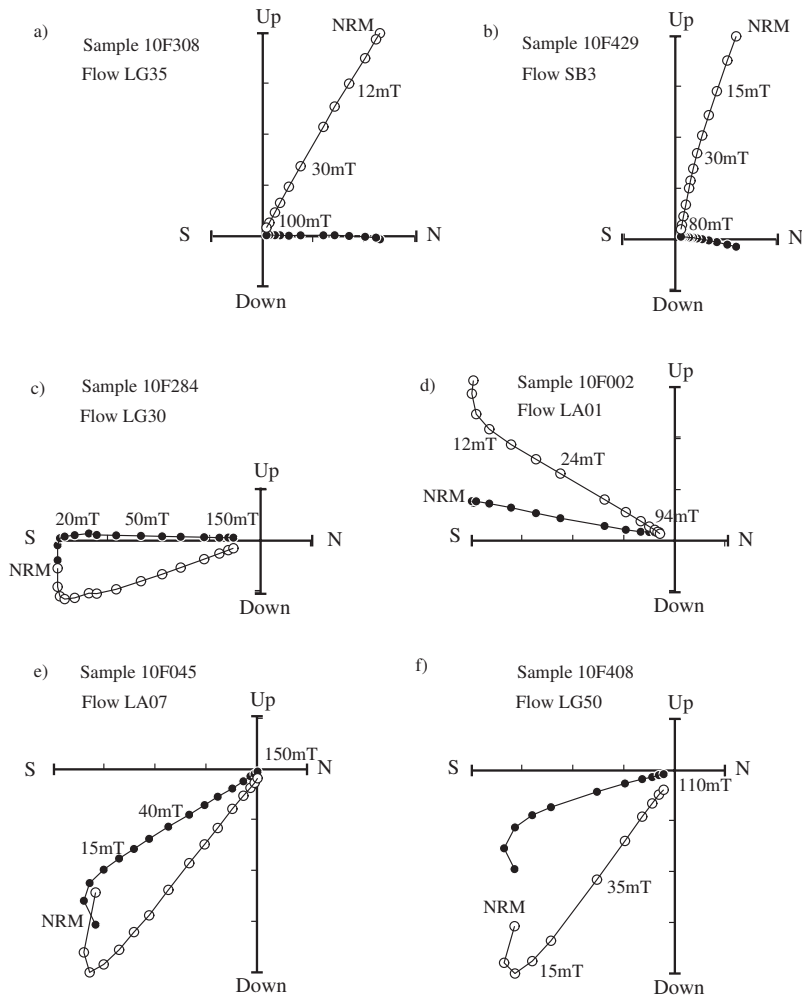


FIGURE 3.4 – Example of representative Zijderveld diagrams of progressive AF demagnetizations for normal (a,b), transitional (c,d), and reversed (e,f) directions. Projections are in geographical coordinates. Solid (open) symbols represent projections into horizontal (vertical) planes.

behaviour in Thellier experiments. Nevertheless, the multispecimen method (Dekkers and Böhnel, 2006; Fabian and Leonhardt, 2010; Muxworthy et al., 2011) enables to determine paleointensities on multidomain grains. Both methods require a good knowledge of the nature, the size and the thermal stability of the magnetic carriers present in the rocks in order to select the adapted samples for each method. That is why we carried out a comprehensive magnetic study on each sampled flow.

### Optical ore microscopy

We performed microscopic observations in reflected light on polished thin section prepared from cylinder cores (Fig. 3.5). We used a Leitz orthoplan microscope which allows a maximum magnification under oil-immersion of 1250x. Fe-Ti oxides and textures were identified according to the Haggerty (1976)'s classification.

## Comportement du champ magnétique lors du renversement d'Akaroa

TABLE 3.1 – Synthetic profile of directions obtained in the three sections sampled. The name of the flow, its position in the section and coordinates are given.  $\nu$  is the viscosity index, n the number of samples used to determinate the direction and N the number of samples available for the flow. Inc and Dec are inclination and declination of the ChRM.  $\alpha_{95}$  is the 95% confidence envelope for the average direction and K is the precision parameter of Fisher distribution. Plat, Plong are the latitude and longitude of the VGP position and Pol is its polarity (N=Normal and R=reverse).

Unity	Alt (m)	Site				Direction		Stat		VGP		
		Coordonnées		$\nu$ (%)	n/N	Inc	Dec	$\alpha_{95}$	K	Plat	Plong	Pol.
LG51	640	43°50'59 S	172°58'12 E	2.02	11/12	51.0	173.5	4.3	113.6	-76.8	328.0	R
LG50	625	43°50'58 S	172°58'12 E	3.83	4/5	51.9	151.4	7.2	163.7	-65.0	280.2	R
LG49	622	43°50'57 S	172°58'13 E	6.16	6/7	48.3	156.6	6.6	104.1	-66.4	293.2	R
LG48	620	43°50'56 S	172°58'13 E	2.42	6/7	50.2	183.0	5.5	148.4	-76.9	4.4	R
LG47	615	43°50'55 S	172°58'12 E	4.87	5/6	55.5	171.9	5.3	212.1	-80.0	311.8	R
LG46	612	43°50'55 S	172°58'12 E	1.57	5/6	53.5	174.8	6.1	159.2	-79.4	328.9	R
LG45	610	43°50'55 S	172°58'12 E	4.85	3/4	58.6	174.8	10.9	128.6	-84.0	310.5	R
LG44	610	43°50'55 S	172°58'12 E	0.81	4/5	55.2	186.5	7.0	173.8	-80.5	26.7	R
LA11	605	43°40'16 S	173°00'38 E	1.82	6/6	32.5	140.6	5.0	181.4	-47.8	288.4	R
LA10	605	43°40'17 S	173°00'36 E	4.75	6/6	64.7	145.9	5.0	181.8	-66.0	244.0	R
LA9	605	43°40'18 S	173°00'35 E	8.59	7/7	32.5	178.2	6.9	78.3	-64.0	349.1	R
LA8	605	43°40'19 S	173°00'35 E	2.45	7/7	43.4	151.6	3.4	318.1	-60.5	292.2	R
LA7	605	43°40'20 S	173°00'33 E	1.79	7/7	41.5	152.6	4.2	210.3	-60.1	295.5	R
LA6	605	43°40'20 S	173°00'32 E	6.31	7/7	40.7	150.4	3.5	293.5	-58.3	293.4	R
LA5	605	43°40'21 S	173°00'30 E	26.2	7/7	34.5	147.7	5.3	129.5	-53.4	295.1	R
LA4	600	43°40'24 S	173°00'27 E	4.62	6/6	53.4	187.2	5.5	151.6	-78.8	025.3	R
LA3	600	43°40'28 S	173°00'23 E	3.44	7/7	62.3	207.4	3.0	412.1	-70.4	092.4	R
LA2	600	43°40'33 S	173°00'17 E	11.2	7/7	-53.0	026.2	5.8	108.5	67.3	245.4	T
LA1	600	43°40'36 S	173°00'13 E	15.3	7/7	-30.8	188.0	4.7	168.2	-29.3	001.8	T
LA0	600	43°40'25 S	172°59'20 E	5.65	4/4	-6.3	290.3	4.2	42.7	16.8	95.0	T
LG43	600	43°50'53 S	172°58'12 E	0.12	5/5	-56.4	23.1	2.9	717.2	71.2	249.4	N
LG42	600	43°50'52 S	172°58'12 E	9.94	6/7	-47.1	24.4	5.3	158.8	65.0	232.5	N
LG41	595	43°50'51 S	172°58'13 E	2.01	6/7	-49.3	19.0	3.7	326.0	69.7	227.1	N
LG40	592	43°50'48 S	172°58'14 E	7.05	7/7	-50.9	24.2	3.8	256.5	67.4	238.3	N
LG39	590	43°50'48 S	172°58'14 E	1.66	7/7	-51.8	23.3	2.8	450.9	68.5	238.7	N
LG38	587	43°50'47 S	172°58'15 E	5.15	7/8	-65.6	6.6	10.4	34.6	83.9	305.9	N
LG37	585	43°50'46 S	172°58'16 E	2.57	6/7	-77.1	328.4	6.2	154.4	62.3	21.0	N
LG36	583	43°50'45 S	172°58'17 E	3.25	7/7	-40.2	347.4	2.7	516.5	66.6	142.5	N
LG35	582	43°50'41 S	172°58'17 E	8.92	8/8	-55.1	5.3	3.9	201.1	81.2	202.2	N
LG34	580	43°50'38 S	172°58'18 E	11.6	4/4	-47.5	0.8	7.4	154.2	74.8	175.6	N
LG33	578	43°50'36 S	172°58'18 E	8.28	7/7	-54.0	6.7	5.5	119.8	79.4	204.3	N
LG32	575	43°50'30 S	172°58'17 E	0.10	2/3	-18.1	151.7	9.4	42.1	-31.0	319.9	T
LG31	570	43°50'29 S	172°58'16 E	11.4	6/7	19.6	181.9	9.7	48.5	-56.2	356.3	T
LG30	560	43°50'29 S	172°58'16 E	0.59	7/7	20.0	181.5	3.5	308.2	-56.4	355.6	T
LG29	540	43°50'26 S	172°58'15 E	6.88	4/7	55.6	176.1	4.0	539.0	-81.7	330.5	R
LG28	530	43°50'24 S	172°58'17 E	15.2	5/5	52.2	184.3	9.8	61.7	-78.5	11.3	R
LG27	525	43°50'24 S	172°58'13 E	1.68	6/8	43.2	179.5	11.0	52.7	-71.3	351.6	R
LG26	520	43°50'22 S	172°58'14 E	1.37	3/3	52.2	165.3	10.0	149.6	-74.1	301.9	R
LG25	517	43°50'20 S	172°58'20 E	6.55	6/7	54.6	162.9	8.5	63.4	-74.2	290.7	R
LG24	515	43°50'20 S	172°58'20 E	18.4	6/7	52.7	173.1	8.9	57.8	-78.2	323.7	R
LG23	512	43°50'19 S	172°58'21 E	5.02	7/7	65.7	148.8	5.5	121.8	-68.0	248.0	R
LG22	510	43°50'18 S	172°58'21 E	4.90	7/7	64.8	150.7	3.6	277.7	-69.3	244.7	R
LG20	507	43°50'16 S	172°58'21 E	4.85	12/12	57.8	172.6	3.3	172.6	-82.2	304.7	R
LG19	505	43°50'10 S	172°58'20 E	11.1	6/6	51.2	183.0	7.9	73.4	-77.8	005.1	R
LG18	502	43°50'07 S	172°58'17 E	8.30	6/6	62.8	190.8	3.9	302.4	-82.2	089.5	R
LG17	500	43°50'03 S	172°58'11 E	6.94	5/9	70.1	171.5	3.3	550.1	-78.3	198.4	R
LG15	490	43°49'58 S	172°58'08 E	5.00	3/4	66.1	218.2	12.9	91.8	-63.4	106.5	R
LG14	480	43°49'57 S	172°58'08 E	0.95	7/7	43.9	158.5	9.6	40.7	-64.8	302.0	R
LG12	465	43°49'52 S	172°58'08 E	3.53	7/7	64.2	188.7	8.0	59.0	-83.5	105.1	R
LG11	460	43°49'52 S	172°58'08 E	14.5	7/7	84.5	240.3	11.4	29.8	-48.4	158.6	R
LG10	440	43°49'50 S	172°58'06 E	17.5	6/7	67.4	156.3	12.7	39.8	-72.7	232.9	R
LG9	420	43°49'48 S	172°58'05 E	7.17	4/6	-35.2	94.3	7.3	50.9	10.3	280.0	T
LG8	375	43°49'41 S	172°57'54 E	1.66	4/7	-47.8	29.1	7.2	161.7	62.4	239.9	T
LG7	360	43°49'40 S	172°57'52 E	1.22	3/3	-74.8	342.4	9.6	166.1	69.5	17.3	T
LG6	350	43°49'38 S	172°57'46 E	1.21	4/8	-21.8	60.4	9.4	116.3	29.0	250.1	T
LG5	205	43°49'09 S	172°57'29 E	3.71	4/7	-52.4	009.1	8.8	109.1	77.1	209.3	N
SB7	310	43°49'17 S	172°59'39 E	33.6	3/3	-45.9	346.8	12.1	105.7	70.3	135.9	N
SB6	300	43°49'23 S	172°59'35 E	4.31	4/4	-36.5	338.5	6.0	236.4	60.5	129.0	N
SB5	295	43°49'22 S	172°59'31 E	22.3	5/6	-45.0	343.6	4.2	339.3	68.2	130.1	N
LG4	190	43°49'09 S	172°57'25 E	10.3	5/7	-57.3	354.2	6.4	141.8	82.6	131.4	N
LG3	170	43°49'07 S	172°57'26 E	9.00	7/7	-49.0	013.0	6.2	96.2	72.7	213.9	N
LG2	165	43°49'06 S	172°57'28 E	1.79	5/5	-47.8	001.6	5.1	222.3	75.0	178.4	N
SB3	160	43°48'88 S	172°59'05 E	22.5	3/3	-81.0	16.8	8.3	219.6	60.3	342.0	N
SB2	130	43°48'74 S	172°58'94 E	9.48	3/4	-64.7	15.1	3.3	1400.4	79.0	283.0	N
SB1	120	43°48'71 S	172°58'88 E	12.3	3/3	-63.9	8.3	9.1	182.9	83.8	282.6	N

### Thermomagnetic experiments

Low-field susceptibility versus temperature experiments (k-T curves) allow to determine the Curie temperature and the stability of the magnetic carriers upon heatings. First, bulk rock was crushed in an agate mortar and sieved to collect the 0.4-0.8 mm

### 3.2.4 Rock magnetism properties

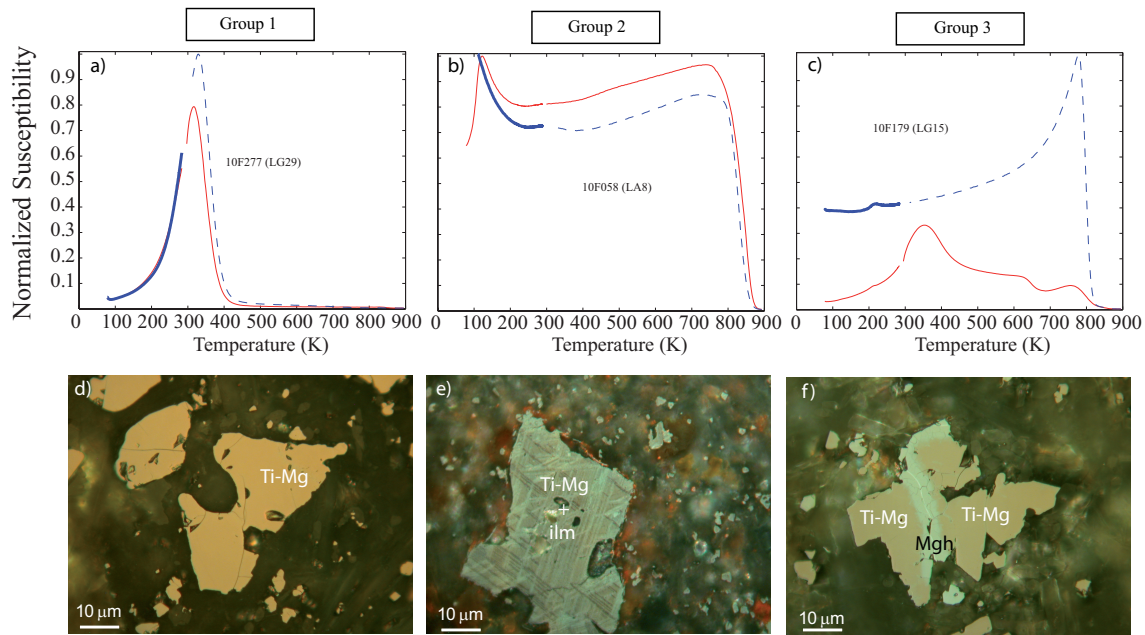


FIGURE 3.5 – Thermomagnetic curves and respected ore microscopic observations carried out under oil immersion in reflected light. *KT* curves at low- and high-temperature in Kelvin for samples 10F277, 10F058 and 10F179. The first heating from liquid nitrogen temperature (78 K) is the thick black curve and the second heating is the fine grey curve. The dashed line is the cooling part of the experiment. d) Homogeneous titano-magnetites (Ti-Mg), e) Exsolved Ti-Mg and ilmenite lamellae (ilm) f) Titano-maghemite (Ti-Mgh) in fractures and Ti-Mg.

size fraction. Then we acquired *k-T* curves at low-temperature by means of a cryostat apparatus (CS-L) and at high-temperature under Argon using a furnace (CS-3) coupled to the KLY-3 Kappabridge instrument (Agico, Czech Republic). At least one sample per flow was first heated from the liquid nitrogen temperature (78 K) to 900 K and cooled down to room temperature. Finally we repeated the low temperature measurements from 78 K up to room temperature to see if any change in susceptibility occurred. The data were corrected for the empty holder and normalized to the maximum susceptibility (Fig. 3.5).

#### First Order Reversal Curves (FORCs)

FORC diagrams (Pike et al., 1999; Roberts et al., 2000) were measured in order to characterize the size of the magnetic carriers. The measurements were carried out at the Laboratoire des Sciences du Climat et de l'Environnement (Gif-sur-Yvette, France) using an Alternating Gradient Magnetometer (AGM) and one sample was measured at the Institut de Minéralogie et de Physique des Milieux Condensés using a Vibrating Sample Magnetometer (VSM). We used an averaging time of 100 ms on the AGM and 20 ms on the VSM and we measured 100 minor loops for each FORC diagram. The smoothing factor (Roberts et al., 2000) was set to 3 for all the FORC diagrams (Fig. 3.6).

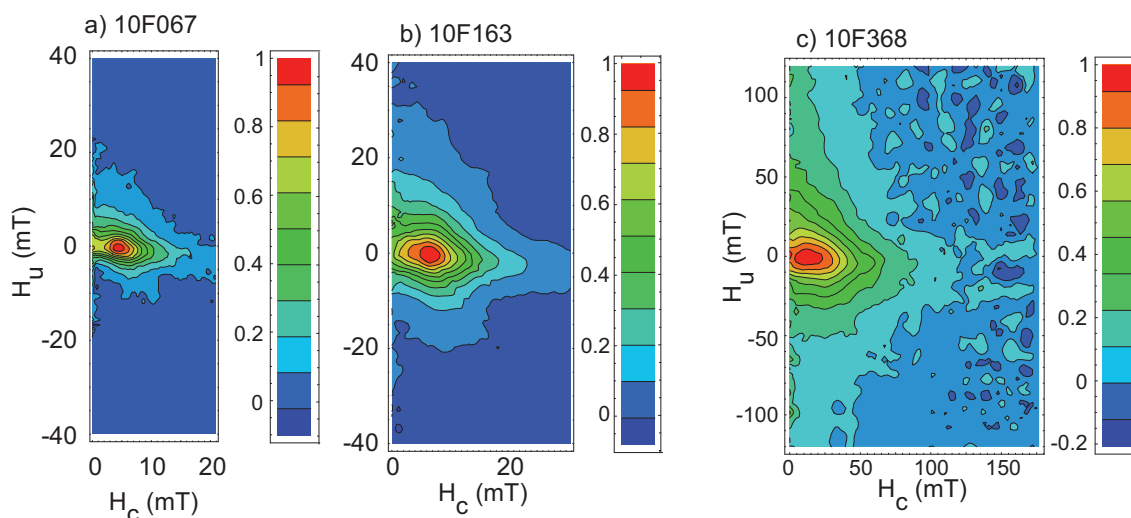


FIGURE 3.6 – FORC diagrams for the three sample. (a) and (b) Samples of MS-type, magnetic grains are a prevalent mixture of MD with a small SD-PSD contribution. (c) T-Type sample in a weak-interacting SD state. The smoothing factor is 3 in each diagram.

## Results

We distinguished three kinds of samples according to their magnetic properties.

**MS-Type** MS-type samples present a single magnetic phase with a low mean Curie temperature in the range 300-400 K (Fig. 3.5, a). The sharp decrease of the magnetic susceptibility at the Curie temperature indicates that the Fe-Ti oxides have a homogeneous chemical composition at the sample scale. Optical microscopy observations (Fig. 3.5, d) show the presence of large titanomagnetite grains (100-150  $\mu\text{m}$ ) that are optically homogeneous up to very large magnifications (stage C1, Haggerty (1976)). Representative FORC diagrams show a coercivity spectrum that does not extend over 40 mT, and a multidomain component is visible through the outermost contours which are almost parallel to the  $H_u$  axis (Fig. 3.6, a and b). The full-width at half maximum (FWHM) for these 2 samples is lower than 16 mT, which indicates small to moderate interactions. Such a magnetic mineralogy seems to be suitable for multispecimen paleointensity experiments. We selected 80 samples from 10 lava flows for paleointensity experiments (25 % of our samples).

**T-Type** T-Type samples show high mean Curie temperatures between about 830 and 850 K, a feature that indicates a pure or nearly pure magnetite composition (Fig. 3.5, b). All samples of this type present a peak in susceptibility at low-temperature around 120 K. According to the experimental work of Senanayake and McElhinny (1982), the low-temperature peak observed in k-T curves is an evidence for a predominance of multidomain (MD) pure or nearly pure magnetite. Such k-T curves are commonly associated

### 3.2.5 Paleointensities

---

to the presence of Ti-poor titanomagnetite subdivided by oxy-exsolved lamellae of ilmenite (Kontny et al., 2003; Camps et al., 2011). Thin section analyses of T-type samples have confirmed the presence of such simple two-phase assemblage corresponding to oxidation stage C3 of Haggerty (1976) (Fig. 3.5, e). FORCs diagrams present spread contours in both  $H_c$  and  $H_u$  directions : the coercivity spectrum extends above 120 mT (the coercivity of the maximum distribution is 18 mT) and the FWHM is 35 mT, which is much higher than for the other samples. Moreover, half the contours do not close up but diverge away from the  $H_c$  axis (Fig. 3.6, c). The behaviour indicates that the magnetization carriers are PSD rather than SD. From these observations, we believe that T-type samples correlate to a mixture of a prevailing fraction of SD/PSD grains and a small fraction of MD grains. Such a magnetic mineralogy seems to be suitable for Thellier-Thellier paleointensity experiments. We selected 57 samples for these experiments (15% of our samples).

**IR Type** In most of the cases, samples clearly present a non reversible behavior for their KT curve (Fig. 3.5, c). Oxidation during the laboratory heatings is unlikely since they were performed under Ar atmosphere. Thus we think that a cation-deficiency which is probably the cause of irreversibility assuming that heating to 600 °C allows few Ti atoms to diffuse into the titano-magnetite lattice, producing a slightly more Ti-rich spinel phase in the cooling curve. Thin section observations show the presence of maghemite (Fig. 3.5, f). This testifies weathering or low-temperature oxidation of titanomagnetites. Hence, a part of the NRM of these samples is undoubtedly of chemical origin. As a consequence, these samples are ill-suited for absolute paleointensity methods and no further investigations have been performed on them. Unfortunately 60% of our samples yield this kind of magnetic mineralogy.

### 3.2.5 Paleointensities

According to the mineralogy of our samples, we applied the Thellier-Thellier's method or the multispecimen protocol.

#### **Thellier Thellier**

**Protocol** Paleointensity measurements were carried out in the laboratory of Geosciences Montpellier, using the Thellier and Thellier (1959) method in its original form with regular partial thermoremanent magnetization checks (pTRM checks). Samples were heated and cooled twice for each temperature step  $T_i$ . At each temperature level  $T_i$ , the samples were heated in zero-field and cooled in an induced field of 50  $\mu$ T, oriented along the  $z$ -axis of the core during the first cooling and in the opposite direction during the second one. Eleven temperature steps were performed from room temperature to

maximum 550°C with decreasing increments as the temperature increases (60-50-30-20 °C). Every two temperature steps a pTRM check was performed to detect any alteration in the pTRM acquisition capacity. All heating-cooling cycles were performed under a vacuum better than  $10^{-2}$  Pa in order to limit possible oxidation during experiment. Each heating-cooling cycle required six to eight hours. Temperature reproducibility between heatings at the same step is within 1 °C. This control is ensured by means of three thermocouples placed at different positions within the heating chamber. The intensity of laboratory field is held with a precision better than  $0.1 \mu\text{T}$ . After each heating/cooling cycle, the remanent magnetization was measured by means of a JR-5A spinner magnetometer. Paleointensity data were interpreted by means of the Thellier Tool software provided by Leonhardt et al. (2004). The statistical parameters used (c.f. Table 3.2) are those proposed by Coe et al. (1978) and modified by Prévot et al. (1985).

**Results** We adopted a standard set of criteria derived from those of Selkin and Tauxe (2000) to select reliable results. First, paleointensity measurements were represented and analyzed by means of Arai diagrams in which the remaining NRM is plotted against the partial TRM acquired after each temperature step of the experiment. We did not use the initial part of these diagrams since it is affected by a secondary magnetization, certainly of viscous origin. The slope of the least-squares-fit line computed from the linear part of these plots gives an estimate of the paleointensity. A value is rejected when the number of selected points is less than four ( $n < 4$ ) or do not span 30 % of the total NRM ( $f < 0.3$ ).

pTRM checks were performed to assess the reliability of a paleointensity estimate. We quantified the difference between two pTRM acquisitions at the same temperature by means of the Difference Ratio (DRAT) parameter. DRAT is expressed in percent and corresponds to the difference measured between repeated pTRM acquisition. The threshold is usually arbitrarily fixed at 10%.

Finally, we checked on the Zijdeveld plots computed from the paleointensity experiments that the NRM fraction used to calculate the paleointensity corresponds effectively to the characteristic remanent magnetization (ChRM) of the sample. The low-temperature part of the NRM may contain natural secondary magnetizations, and chemical remanent magnetization acquired during the experimental heatings may superpose to the NRM if changes occurred in the magnetic minerals. This check is achieved qualitatively by a visual inspection of the vector endpoint diagrams. The points in the selected interval should trend toward the origin.

We applied these criteria and we obtained only 17 reliable values of paleointensity from the 57 samples (9 sites) pre-selected (Tab. 3.2). Representative Arai plots are illustrated in Fig. 3.7. For each lava flow individual paleointensity estimates are coherent as attested by the small standard errors, all being less than 10% of the average, that

### 3.2.5 Paleointensities

TABLE 3.2 – *Thellier-Thellier paleointensity results.  $F$  is the paleointensity and  $\Sigma$  the standard error.  $N$  is the number of points in the interval of temperature  $T_{\min}$ - $T_{\max}$  used to determine the paleointensity.  $f$  is the NRM fraction used to determine the peointensity,  $g$  the gap factor,  $q$  the quality factor and  $w$  the weighting factor. DRAT corresponds to the difference ratio between repeat pTRM steps normalized  $F_m$  is the mean weighted paleointensity for each site calculated using  $1/\sigma^2$  as the weighting parameters. Uncertainties around the estimate of the means are quoted with standard errors*

Sample	F	$\sigma$	Tmin	Tmax	n	f	g	q	w	Drat	$F_m \pm \sigma$ ( $\mu$ T)
LG44											$84.6 \pm 14.4$
10F374C	69.7	1.97	150	510	9	0.38	0.85	11.6	4.4	1.9	
10F374B	72.5	2.27	225	510	8	0.37	0.84	9.9	4.1	4.8	
10F373B	96.0	2.85	150	510	9	0.40	0.86	11.7	4.4	2.3	
10F372B	104.4	4.94	150	510	9	0.48	0.86	8.7	3.3	3.0	
LG43											$71.4 \pm 3.7$
10F369C	73.7	3.40	150	510	9	0.57	0.86	10.6	4.0	1.3	
10F368D	74.1	4.28	150	510	9	0.59	0.85	8.7	3.3	1.6	
10F367C	65.2	2.94	150	510	9	0.67	0.85	12.6	4.8	4.2	
10F367B	70.4	2.93	150	510	9	0.65	0.85	13.3	5.0	3.4	
10F366B	76.1	4.67	150	510	9	0.60	0.85	8.4	3.2	3.5	
10F365B	72.7	5.48	150	480	8	0.38	0.82	4.2	1.7	4.3	
LA8											$15.3 \pm 1.9$
10F056C	14.3	1.83	150	510	9	0.44	0.82	2.9	1.1	9.9	
10F054B	18.2	0.68	150	510	9	0.46	0.85	10.6	4.0	4.7	
10F053C	13.8	0.37	150	550	11	0.61	0.84	19.1	6.4	9.0	
10F052B	15.2	1.25	150	510	9	0.48	0.83	4.8	1.8	6.2	
LA7											$35.4 \pm 7.4$
10F051C	33.4	1.36	150	510	9	0.50	0.84	10.2	3.9	4.4	
10F050B	45.7	2.37	150	480	8	0.49	0.85	8.0	3.3	7.9	
10F048B	27.5	1.41	150	510	9	0.52	0.86	8.7	3.3	5.1	

comforts the reliability of our results. However, the quality factors are very scattered (2.2 to 19). Hence, we calculated a weighted average and a standard error average for each phase, using the weighting by the standard error as recommended by Coe et al. (1978) (eq. (4) and (5)). The irreversibility of the magnetic properties is generally observed after heating at 500 °C.

### Multispecimen

**Protocol** The multispecimen parallel differential pTRM method has been first developed by Dekkers and Böhnell (2006) (denoted here as MSP-DB). This method has a large potential to improve absolute paleointensity determination because it can be applied on samples yielding a multidomain behavior. The basic idea of the method relies on the the first-order symmetry properties of pTRM in MD grains (Biggin and Poidras, 2006). An artificial pTRM is overprinted on the direction of the initial TRM during a single heating at a temperature  $T_h$ . It is assumed that the final remanence is smaller than the initial TRM if  $H < H_0$  and larger when  $H > H_0$ . However Michalk et al. (2008, 2010) showed experimentally that this method clearly overestimates the paleointensity. Fabian and Leonhardt (2010) developed a new protocol denoted as multispecimen domain correction state (MSP-DSC). The varying NRM fraction  $f$  replaced by the pTRM\*( $T_h$ ) leads to considerable scatter in the MSP-DB method. To avoid this biasing effect, the actually

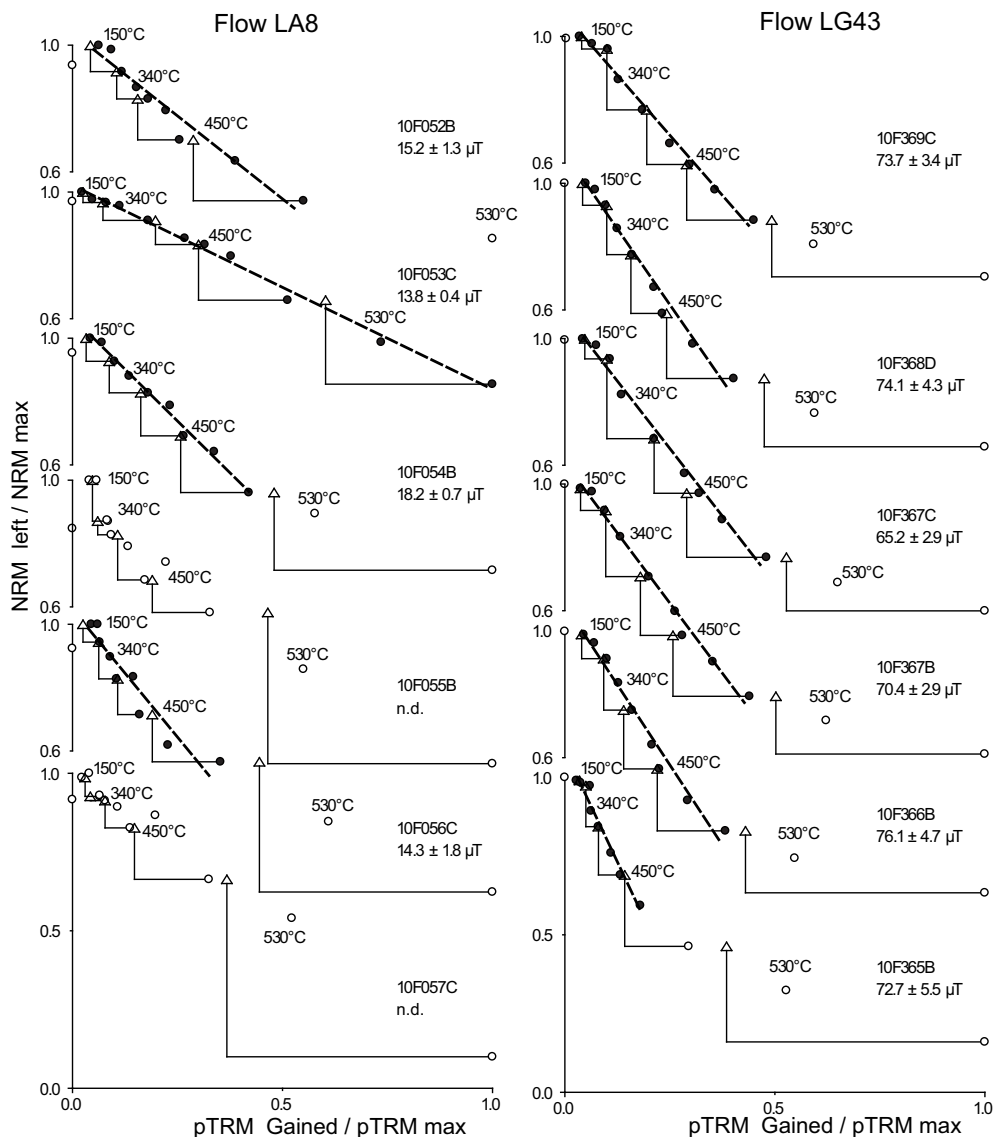


FIGURE 3.7 – Composite Arai diagrams for samples (a) from flow LA8, left column, and (b) from flow LG 43, right column. Solid (open) circles are NRM-TRM points accepted (rejected) to calculate the least squares line used to estimate the paleointensity. Triangles denote the pTRM checks. NRM and TRM are normalized by the NRM max and TRM max, respectively.

overprinted pTRM\*( $T_h$ ) is normalized by  $f$ . Moreover, a correction of the domain state is also proposed in this protocol. We used this new approach to increase the number of paleointensities on MS-type samples. First we determined a temperature  $T_v$  according to the temperature spectrum and Zijderveld diagrams to remove the viscous overprint or any secondary component. For few samples yielding a small IRM an AF pre-treatment was performed until maximum 10 mT in order to work on a pure TRM. Then the heating temperature  $T_h$  was chosen freely, sufficiently high to work on a sufficient fraction of the TRM (at least 30 %) but sufficiently low to avoid chemical alteration. Finally we performed five measurements on each specimen according to the Fabian and Leonhardt

### 3.2.5 Paleointensities

(2010)'s protocol :

1. The original TRM  $m_0$ (after thermal cleaning to  $T_v$ )
2. Remanence  $m_1$  after an in-field heating-cooling cycle to  $T_h$ , where the applied laboratory field  $H_{lab}$  is aligned parallel to  $m_0$ .
3. Remanence  $m_2$  after an in-field heating-cooling cycle to  $T_h$ , where the applied laboratory field  $H_{lab}$  is aligned anti-parallel to  $m_0$ .
4. Remanence  $m_2$  after a zero-field heating to  $T_h$ , and cooling in the applied laboratory field  $H_{lab}$ , aligned parallel to  $m_0$ .
5. Remanence  $m_4$ , after repeating the step 2.

After each eating-cooling cycle, each specimen was heated until  $T_v$  in a zero-field furnace.

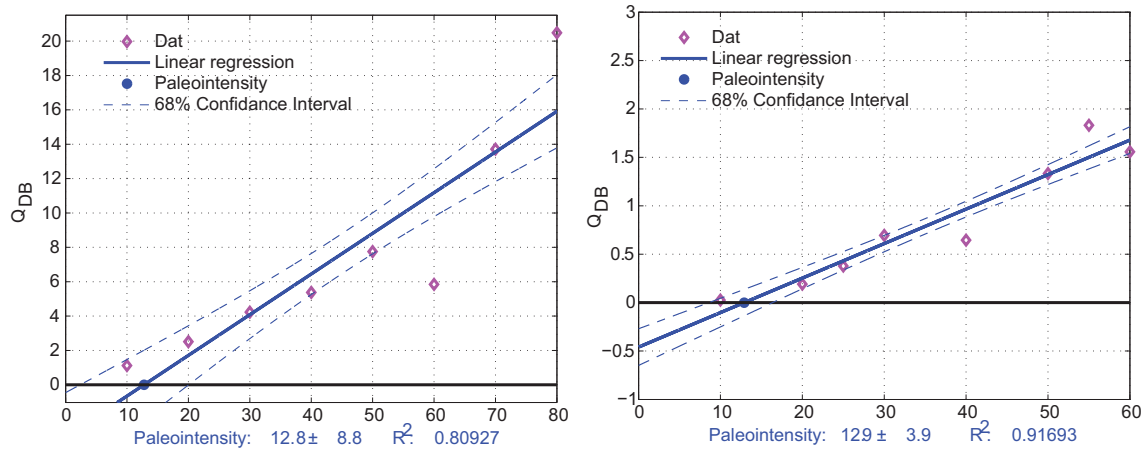


FIGURE 3.8 – Application of the Dekkers and Böhnel (2006)'s protocol on samples from lava flow LA3.  $Q_{fc}$  is plotted against the applied field.

**Results** For each flow we calculated  $Q_{db}$ ,  $Q_{fc}$  and  $Q_{dsc}$  (Fabian and Leonhardt, 2010). Unfortunately no  $Q_{dsc}$  were estimated. Indeed, we encountered the same problem as Muxworthy et al. (2011), for all of our flow we found  $\alpha = 0$ . Moreover, for few flows no paleointensities were estimated using  $Q_{fc}$ . Thus, we only present the  $Q_{db}$  results. For each flow we plotted  $Q_{db}$  against the applied field (Fig. 3.8). All paleointensity estimates are gathered in Tab. 3.3. We applied the approach of other earlier studies (Dekkers and Böhnel, 2006; Michalk et al., 2008, 2010; Muxworthy et al., 2011) to determine the error by calculating the confidence intervals at 68 per cent to the linear fits.

All paleointensity estimates present a low value, between 6.4 and 18.7  $\mu\text{T}$ , but all linear regressions show a relatively good correlation coefficient greater than 0.84, excepted the flow LG45.

TABLE 3.3 – *Paleointensity estimates from Dekkers and Böhnel (2006)'s method.*

Location	PI estimate ( $\mu\text{T}$ )	$\sigma$ ( $\mu\text{T}$ )	Corrélation coefficient R
LG48	12.5	4.4	0.832
LG45	18.7	6.9	0.634
LA3	12.4	3.8	0.847
LA2	10.1	3.2	0.982
LA1	12.8	8.1	0.809
LG42	6.4	4.9	0.882
LG40	16.7	4.5	0.953

### 3.2.6 Discussion

Our directional results suggest the record of two successive reversals N-T-R-T-N-T-R in agreement with the former studies carried out by Evans (1970) and Hoffman (1986). The transitional VGPs obtained in this study seem to show two longitudinal preferences, through Americas and Australia according to Hoffman (1986) (Fig. 3.9). This observation supports a possible configurational persistence consistent with long-lived mantle control over the pattern of dynamo flux. Our results and those of Hoffman et al. (2008) on Australian lava flows suggest that the characteristic time for invariant control by the mantle over flux emerging from the outer core is at least on order of a few tens of million years. The availability of transitional paleomagnetic data from still older times may help to delineate this duration and, to understand changes in the pattern of long-standing concentrations of magnetic flux at the core-mantle boundary and the role played by the mantle on the dynamo process (Olson et al., 2010).

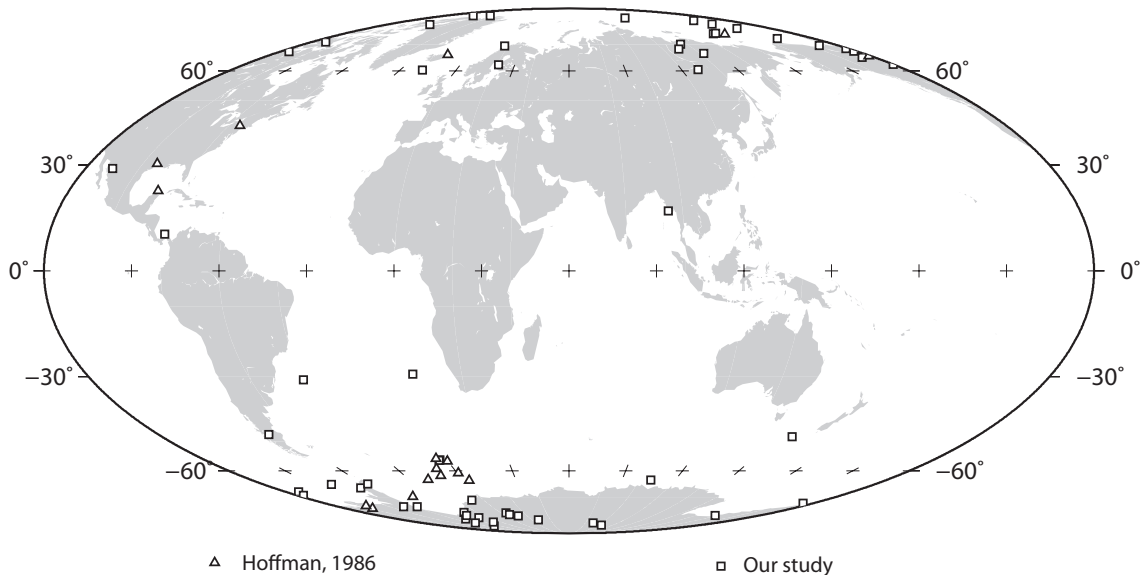


FIGURE 3.9 – *Location of the VGP for each sampled flow for our study (squares) and for the Hoffman (1986)'s study (triangles).*

We obtained in addition very few but reliable paleointensities for transitional, reverse and normal polarities. Most of the estimated paleointensities have an extremely low value

### 3.2.6 Discussion

(about  $15 \mu\text{T}$ ) and are located at the top of the section, during a short polarity change. Moreover, the Ar/Ar ages determined by Timm et al. (2009) show that Akaroa volcano was active from 9.4 Myrs to 8.8 Myrs. The Ar/Ar age determined on the top of our section is  $9.37 \pm 0.42$  Myrs, that corresponds to the earlier phase of the activity. We can conclude that the whole sequence was erupted in a very short time and that all lava flows are more or less contemporaneous. The correlation of the section polarity with the geomagnetic time scale (Ogg and Smith, 2004) and the estimated age of the section allows to conclude that the sequence recorded the C4Ar1.n-C4Ar1.r reversal (Fig. 3.10). According to all these observations, we suggest that the brief polarity change at the top of the section corresponds to a geomagnetic rebound occurring during the transitional phase of the reversal before stabilizing.

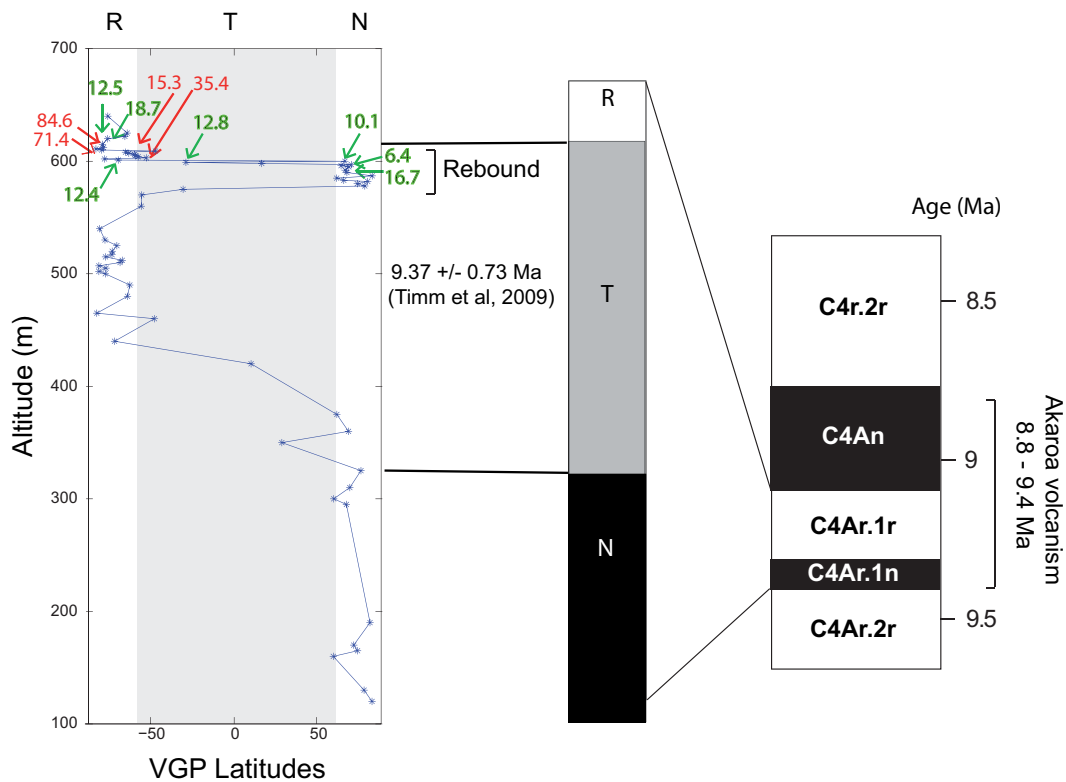


FIGURE 3.10 – Synthetic profile of the three sections sampled with VGP latitudes calculated for each flow. Shading denotes latitudes  $< \pm 60^\circ$ , which corresponds to transitional flows. Correlation of the section polarity with geomagnetic time scale (Ogg and Smith, 2004) is done with the help of the age determined for the section by Timm et al. (2009).

The rock magnetic study has shown that most of the samples from this sequence yield a predominant population of multidomain grains or present a maghemitization. Both mineralogies are not suitable to determine absolute paleointensity, including with the Shaw method. However, no information on the samples mineralogy are available from the Sherwood and Shaw (1986)'s study and we have no geological indications to replace Sherwood and Shaw (1986)'s paleointensities in the sequence to compare them with

our values. Thus it is difficult to have a clear conclusion on this point. However these paleointensities are not totally in disagreement with our results. Our paleointensities estimated during the geomagnetic rebound have more or less the same intensity with low values between 6 and 20  $\mu\text{T}$  whatever is the polarity, that does not contradict the Sherwood and Shaw (1986)'s results.

### **3.2.7 Conclusion**

Our comprehensive paleomagnetic studies of the volcanic sequence from the Akaroa sequence in Banks peninsula, New Zealand, leads to the following conclusions :

1. Stratigraphic correlations between the three overlapping profiles studied in the present survey are established by means of the direction of the remanent magnetization, rock magnetism properties, mineralogy and field observations.
2. The directional results show a complete sequence of N-T-R-N-T-R polarity and are in agreement with the previous work of Evans (1970); Hoffman (1986).
3. We estimated paleointensities using the multispecimen protocol and the Thellier-Thellier method according to rock magnetic properties of the samples. These paleointensities are extremely low at the top of the sequence (around 15  $\mu\text{T}$ ) during the second reversal and very high at the end of the sequence.
4. We assume that this second polarity change at the top of the section could be a geomagnetic rebound. First, this interpretation relies on the low paleointensity value during this event. Second, the geochronological ages suggest that the entire sequence was erupted in a very short time, during the early phase of Akaroa volcanic activity at about 9.37 Ma. Thus, we conclude that this sequence corresponds to the record of a single complex reversal corresponding to the C4Ar1.n-C4Ar1.r reversal according to the geomagnetic time scale.